

The electronic structure of $R\text{NiC}_2$ intermetallic compounds

J. Laverock, T. D. Haynes, C. Ulfeld and S. B. Dugdale
*H. H. Wills Physics Laboratory, University of Bristol,
 Tyndall Avenue, Bristol BS8 1TL, United Kingdom*

First-principles calculations of the electronic structure of members of the $R\text{NiC}_2$ series are presented, and their Fermi surfaces investigated for nesting propensities which might be linked to the charge-density waves exhibited by certain members of the series ($R = \text{Sm, Gd and Nd}$). Calculations of the generalized susceptibility, $\chi_0(\mathbf{q}, \omega)$, show strong peaks at the same \mathbf{q} -vector in both the real and imaginary parts for these compounds. Moreover, this peak occurs at a wavevector which is very close to that experimentally observed in SmNiC_2 . In contrast, for LaNiC_2 (which is a superconductor below 2.7K) as well as for ferromagnetic SmNiC_2 , there is no such sharp peak. This could explain the absence of a charge-density wave transition in the former, and the destruction of the charge-density wave that has been observed to accompany the onset of ferromagnetic order in the latter.

PACS numbers: 71.45.Lr, 71.18.+y

I. INTRODUCTION

The idea that the Fermi surface (FS), through instabilities in the electronic structure (such as nesting features or van Hove saddle points), can drive low-dimensional systems into new ground states such as spin-density or charge-density waves (CDW), is well-known (for example, the transition metal dichalcogenides [1] and Cr [2]). More recent theoretical studies of the role of the FS in CDW formation [3, 4] have contributed greatly to our understanding of the phenomenon, and have clarified a number of misconceptions. Specifically, those authors emphasize that simply inspecting the FS for possible nesting features without actually calculating the real part of the electronic susceptibility does not help in predicting CDW instabilities [4]. They further urge caution about attributing such nesting as the only (or even main) driving force for such instabilities. In this paper we calculate the electronic structure, FS and susceptibilities of several members of the $R\text{NiC}_2$ family which have been shown to exhibit a fascinating array of electronic instabilities [5, 6]. SmNiC_2 has recently been found to host an interesting interplay between CDW and ferromagnetic order [7]. On cooling below a temperature of 148K, a resistivity anomaly and the appearance of satellite peaks in x-ray scattering indicate the formation of a CDW. The critical phonon softening, inferred from the thermal diffuse scattering above 148K (and which also disappears at the ferromagnetic transition) occurs at two specific wavevectors, namely $\mathbf{q}_1 = (0.5, 0.52, 0)$ and $\mathbf{q}_R = (0.5, 0.5, 0.5)$ [7]. Of these two wavevectors, it is the incommensurate \mathbf{q}_1 modulation which develops into a CDW. Below 17.7K the satellite peaks suddenly disappear and there is a sharp decrease in the resistivity, and both phenomena are coincident with the appearance of ferromagnetic order [7]. Shimomura *et al.* tentatively suggest that the diffuse scattering associated with the phonon softening, the formation of the CDW state and their disappearance at the (first order) ferromagnetic transition could be collectively understood from a knowledge of the FS of

SmNiC_2 [7]. In this paper we address this issue through *ab initio* calculations of the electronic structure of the $R\text{NiC}_2$ system.

II. ELECTRONIC STRUCTURE CALCULATIONS

The $R\text{NiC}_2$ family possess the orthorhombic CeNiC_2 structure (Space Group 38, *Amm2*) [8], which is shown in Fig. 1a. The electronic band structure of $R\text{NiC}_2$ was calculated for several R (La, Nd, Sm and Gd) using the scalar-relativistic linear muffin-tin orbital (LMTO) method within the atomic sphere approximation (ASA) including combined-correction terms [9]. Here, the potential is described within the local density approximation for non-magnetic calculations [10] and the lo-

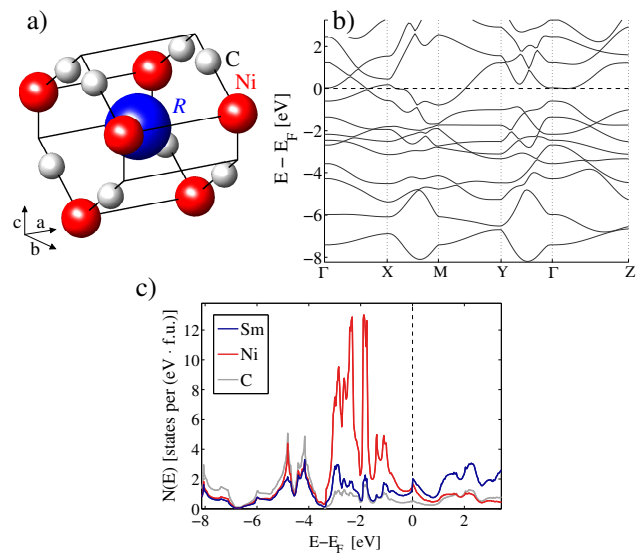


FIG. 1: (color online) The (a) crystal structure, (b) electronic band structure, and (c) density of states of SmNiC_2 .

R	a (Å)	b (Å)	c (Å)	Ref.	$N(E_F)$ [states per (eV · f.u.)]
La	3.956	4.563	6.204	[12]	4.34
Nd	3.765	4.544	6.146	[12]	2.64
Sm	3.703	4.529	6.098	[13]	3.84
Gd	3.649	4.518	6.077	[12]	4.28

TABLE I: Lattice parameters used in the electronic structure calculations, accompanied by the references from which they were taken. The density of states at the Fermi level, $N(E_F)$, obtained from the calculations, is also given.

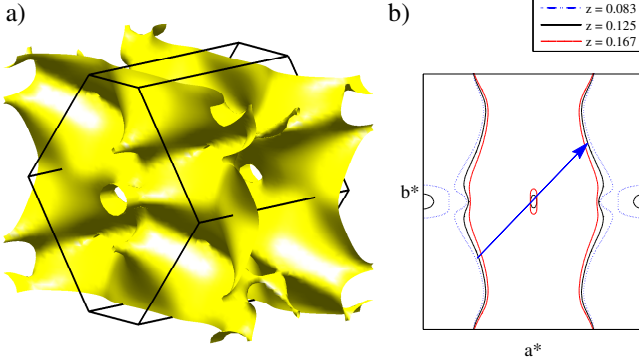


FIG. 2: (color online) The FS of SmNiC_2 , (a) in 3D with the first Brillouin zone marked, and (b) several contours in planes perpendicular to c^* . The arrow in (b) denotes the experimentally observed CDW wavevector $\mathbf{q} = (0.5, 0.52, 0)$. All units are in terms of $2\pi/(a, b, c)$.

cal spin density approximation for spin-polarized calculations [11]. The lattice constants used in the calculations are shown in Table I. All calculations included a basis of s , p , d and (for Ni and R) f states; self-consistency was achieved at 1099 k-points in the irreducible $(1/8)^{\text{th}}$ wedge of the BZ (corresponding to a mesh of $13 \times 13 \times 13$ in the full BZ). The localized rare-earth f -electrons were described using the open-core method, in which they are treated as partially-filled core states.

The electronic band structure and density of states of SmNiC_2 are shown in Fig. 1b and Fig. 1c, respectively. The FS, shown in Fig. 2, comprises a single sheet, originating from hybridized states of predominantly rare-earth / nickel d -character. A closer look at the FS reveals that it indeed has strong potential for nesting. In Fig. 2b, a contour of the FS at several slices through constant c^* is shown, with the arrow indicating a nesting vector of $(0.5, 0.52, 0)$. In order to further investigate the role of nesting, the non-interacting susceptibility was investigated. Neglecting matrix elements, the non-interacting susceptibility, $\chi_0(\mathbf{q}, \omega)$ for wavevector \mathbf{q} and frequency ω can be expressed as:

$$\chi_0(\mathbf{q}, \omega) = \sum_{nn', \mathbf{k}} \frac{f(\epsilon_{n, \mathbf{k}}) - f(\epsilon_{n', \mathbf{k}+\mathbf{q}})}{\epsilon_{n, \mathbf{k}} - \epsilon_{n', \mathbf{k}+\mathbf{q}} - \omega - i\delta}, \quad (1)$$

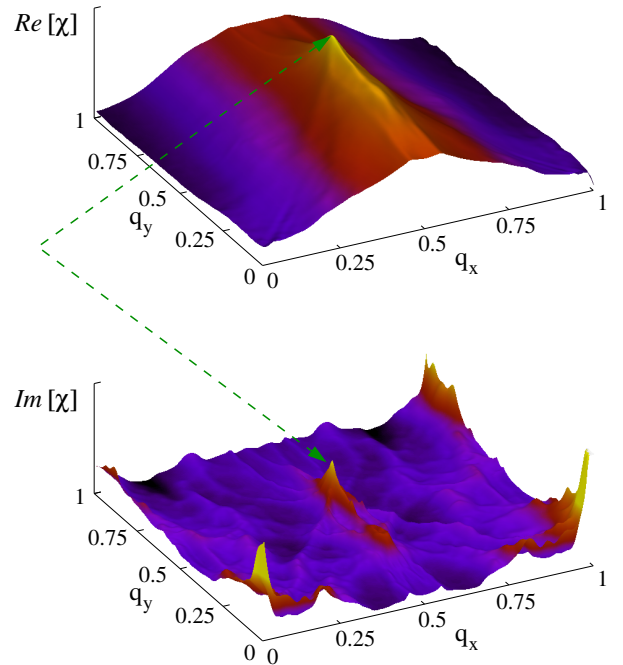


FIG. 3: (color online) $\chi_0(\mathbf{q})$ for SmNiC_2 . The arrow denotes the peak in both real and imaginary parts of $\chi_0(\mathbf{q})$ at $\mathbf{q} = (0.5, 0.56, 0)$.

where $f(\epsilon)$ is the Fermi function and the sum runs over bands n and n' through the Brillouin zone. The Brillouin zone integration is performed using the tetrahedron method of Rath and Freeman [14]. As recently emphasized by Johannes *et al.*, although the imaginary part of $\chi_0(\mathbf{q})$ depends only on details of the electronic structure near the Fermi energy, it is the *real* part of $\chi_0(\mathbf{q})$ (which has contributions coming from a bandwidth-sized window of energies) that could indicate a CDW instability [4]. Both the real and imaginary parts of the non-interacting susceptibility were calculated for SmNiC_2 , and are shown in Fig. 3. It is noteworthy that there is a strong peak at the same \mathbf{q} vector in both the real and imaginary parts of $\chi_0(\mathbf{q})$. Closer inspection reveals that the peak is at a wavevector of $(0.5, 0.56, 0)$, which is very close to the CDW vector \mathbf{q}_1 identified by Shimomura *et al.* [7]. It should be borne in mind when comparing the experimental \mathbf{q}_1 and theoretical peak in $\chi_0(\mathbf{q})$ that our calculations have been performed at the experimental lattice constant, rather than at the energy minimum of the LMTO calculation. Nevertheless, excellent qualitative, and good quantitative agreements are found between experiment and these band structure calculations. Approximations beyond the ASA (such as full-potential schemes) and a fully-relativistic treatment may also improve the precise location of the peak in $\chi_0(\mathbf{q})$, and its agreement with the experimental \mathbf{q}_1 . The $\chi_0(\mathbf{q})$ was also

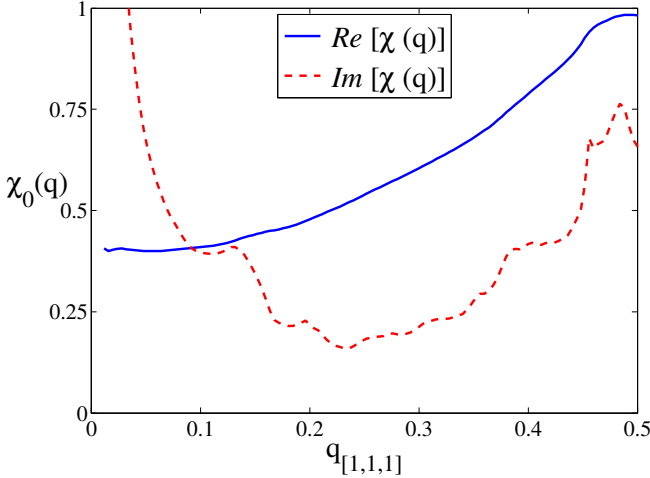


FIG. 4: (color online) Real and imaginary parts of $\chi_0(\mathbf{q})$ along the $[1, 1, 1]$ direction, showing the peak at $\mathbf{q}_R = (0.5, 0.5, 0.5)$ associated with the thermal diffuse scattering observed by Ref. [7]. Owing to the crystal structure, there is a symmetry axis at $q_{[1,1,1]} = (0.5, 0.5, 0.5)$.

calculated along the $[1, 1, 1]$ direction (shown in Fig. 4) and again a peak was found at a vector of $(0.5, 0.5, 0.5)$, which matches the \mathbf{q}_R vector associated with the thermal diffuse scattering by Shimomura *et al.* [7].

Calculations for both NdNiC_2 and GdNiC_2 reveal similar electronic structure and Fermi surfaces to the Sm compound, and the nesting properties already identified for SmNiC_2 are still present in a visual inspection of the FS. Furthermore, calculations of both the real and imaginary parts of $\chi_0(\mathbf{q})$ show comparable structure, the strong peak previously identified for the Sm compound developing in $Re[\chi(\mathbf{q})]$ for $\mathbf{q} = (0.5, 0.55, 0)$ and $\mathbf{q} = (0.5, 0.57, 0)$ for NdNiC_2 and GdNiC_2 , respectively (see Fig. 5). Both the Nd and Gd compounds exhibit anomalies in the resistivity that have been identified with the emergence of a CDW [5]. Although the wavevectors that define these CDW states have not yet been investigated, these results suggest the CDW structure is expected to be similar in nature to that already observed for SmNiC_2 , with a weak dependence on the particular rare-earth compound (presumably associated with the lanthanide contraction). The coincidence of the peak structure in both the real and imaginary parts of the susceptibility for several different rare-earths, demonstrated in Fig. 5, underlines the importance of the FS (through nesting) in these systems.

Conversely, LaNiC_2 shows no equivalent kink in its resistivity [5] for temperatures down to 12K, raising the question of whether this compound shares the same FS topology, and more specifically, whether the same nesting feature is present. We have addressed this by calculating the electronic structure and $\chi_0(\mathbf{q})$ for LaNiC_2 . The density of states at the Fermi level is shown in Table I, alongside comparative values for the other rare-earth compounds addressed in this study. The FS, shown

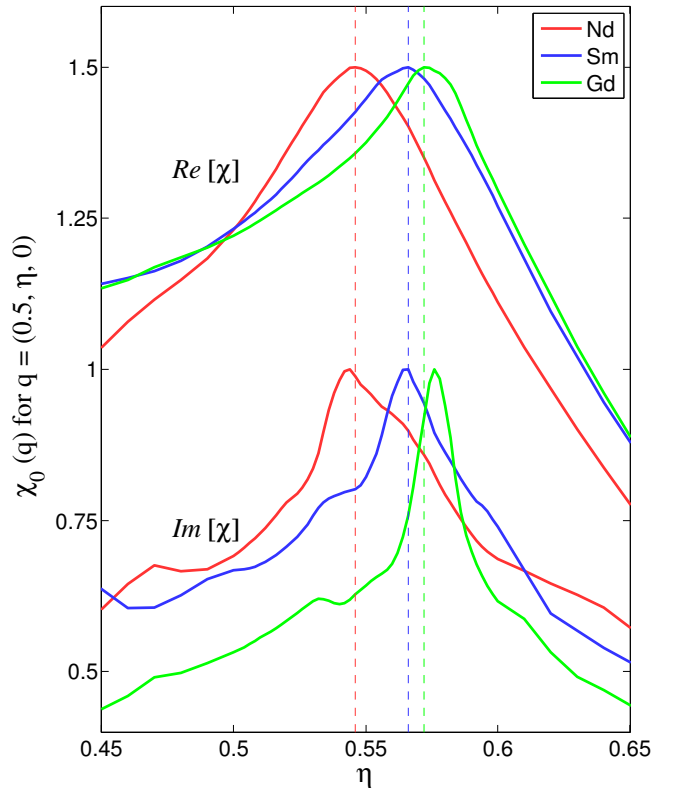


FIG. 5: (color online) The real (top) and imaginary (bottom) parts of $\chi_0(\mathbf{q})$ for different rare-earth elements (Nd, Sm and Gd), shown along the $\mathbf{q} = (0.5, \eta, 0)$ direction as a function of η . The dashed vertical lines indicate the location of the peaks in the real part of the susceptibility for each rare-earth.

in Fig. 6b, is found to be topologically quite different, and the features of the FS that give rise to the nesting in SmNiC_2 appear strongly distorted, as demonstrated by the constant c^* contours shown in Fig. 6c. The $Im[\chi_0(\mathbf{q})]$ shows a broad series of ripples along the $\mathbf{q} = (0.5, \eta, 0)$ direction (see Fig. 7), rather than the strong peak observed for SmNiC_2 , compounding the evidence of poor nesting. In the real part of the susceptibility, also shown in Fig. 7, the peak becomes spread out over some $\sim 0.4b^*$ of the Brillouin zone, which is unlikely to drive a CDW. Calculations for SmNiC_2 in the LaNiC_2 structure yield similar results, emphasizing that the transition of the FS from strong to weaker nesting is a consequence of the structure, rather than the particular rare-earth substitution.

Spin-polarized calculations of the electronic structure have also been performed for SmNiC_2 in order to investigate whether a similar transition in the nesting qualities of the FS (as a consequence of the spin-splitting of the FS) can explain the disappearance of the CDW state that accompanies the onset of ferromagnetism. These calculations have been performed at the same lattice constant used for non-magnetic SmNiC_2 , since the structural transition that has been reported at the Curie temperature

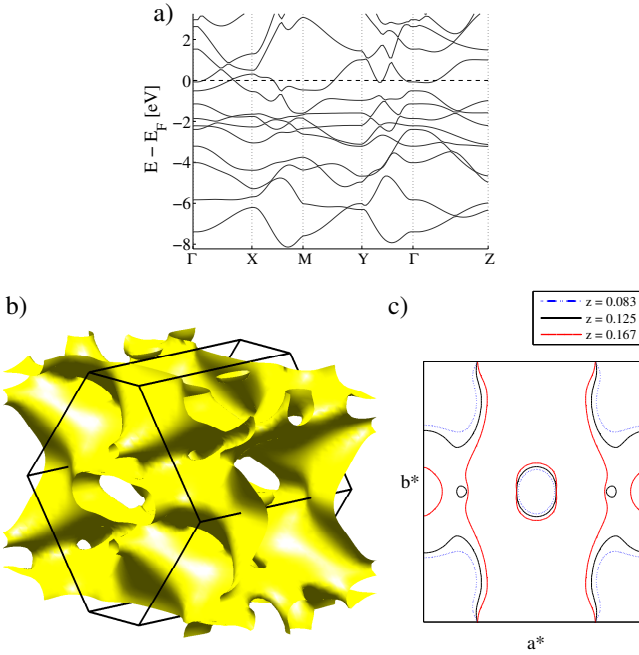


FIG. 6: (color online) The electronic band structure (a) and FS of LaNiC_2 , (b) in 3D with the first Brillouin zone marked, and (c) several contours as for Fig. 2.

[5] is small and does not break any additional symmetry. Although a total ordered moment of $0.32\mu_B$ is reported experimentally [13], the magnetic state of the localized Sm f electrons has not yet been clarified. Measurements of X-ray Magnetic Circular Dichroism on the K -edge of Ni in SmNiC_2 at 5K have indicated that there is a finite moment on the Ni site [15], but a full analysis of the moment was not possible. In our calculations, a spin moment of $0.17\mu_B/\text{Sm}$ develops, which is about half that reported experimentally, and is predominantly located on the Ni site. Inspection of the ferromagnetic FS suggests that the different band filling in the majority sheet substantially weakens the nesting, but it still remains to some extent in the minority FS. Calculations of $\chi_0(\mathbf{q})$ reveal a strong suppression of the $(0.5, \eta, 0)$ peak in the imaginary part, whereas its real counterpart displays a broad ridge over a large range of η , which would again be unlikely to drive a CDW instability. Additional calculations at a fixed spin moment that corresponds to the (total) experimental magnetic moment reveal this effect is even stronger, and the broadening of the ridge structure in the real part of $\chi(\mathbf{q})$ is spread over almost half the Brillouin zone in the $(0.5, \eta, 0)$ direction.

III. CONCLUSION

We have calculated the FS of several (La, Nd, Sm and Gd) members of the $R\text{NiC}_2$ series, accompanied by calculations of both real and imaginary parts of the non-interacting susceptibility $\chi_0(\mathbf{q})$. For the Nd, Sm and Gd

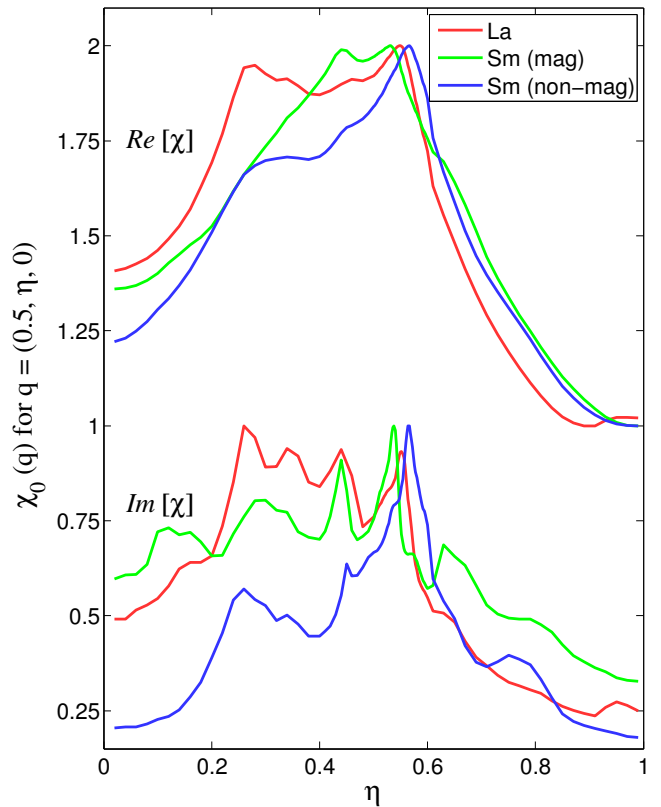


FIG. 7: (color online) Real (top) and imaginary (bottom) parts of $\chi_0(\mathbf{q})$ for LaNiC_2 and ferromagnetic SmNiC_2 (at the LMTO moment of $0.17\mu_B$). For comparison, the $\chi_0(\mathbf{q})$ for non-magnetic SmNiC_2 shown in Fig. 3 is reproduced here. Note the broad hump in $\chi_0(\mathbf{q})$ for both LaNiC_2 and ferromagnetic SmNiC_2 , in contrast to the sharp peak shown in Fig. 3 for non-magnetic SmNiC_2 .

members, peaks in the imaginary part of χ_0 , that can be directly identified with corresponding nesting properties of the FS, still persist in the real part of χ_0 , which is the relevant quantity for a CDW instability. The wavevector $[0.5, \eta, 0]$ corresponding to these peaks in $\chi_0(\mathbf{q})$ is close ($\eta = 0.56$) to the experimental wavevector ($\eta = 0.52$) obtained from x-ray scattering measurements of SmNiC_2 [7]. On the other hand, the FS of LaNiC_2 is found to be markedly different, and the $\chi_0(\mathbf{q})$ does not exhibit such strong structure, providing a possible route towards explaining the apparent absence of a CDW state for this particular compound. Spin-polarized calculations for SmNiC_2 at two different magnetic moments (0.17 and $0.32\mu_B$) demonstrate the gradual destruction of the nesting properties of the FS with increasing moment. The strong peak in $\chi_0(\mathbf{q})$ that is present at zero moment becomes washed out as the spin-polarized bands separate, in agreement with the suggestion of Shimomura *et al.* that the ferromagnetic transition in this compound adversely affects the nesting properties of the FS and leads to a destruction of the CDW state [7].

In summary, our findings suggest that for the Sm, Gd

and Nd compounds, the FS does indeed nest at the CDW wavevector recently observed for SmNiC_2 , and more importantly, this strong divergence survives in the real part of the susceptibility. Furthermore, calculations of two isostructural compounds for which CDW formation has not been observed show substantially weaker divergences in their respective susceptibility, lending support to the idea that FS nesting plays an important role in deciding the fate of these systems.

Note added during revision

During the preparation of this manuscript, a recent study of the electronic structure of LaNiC_2 has been re-

ported [16], in which the authors have relaxed the internal crystal structure. They go on to comment that the FS they obtain is in excellent agreement with our results. In response to their investigation, we have repeated the calculation of LaNiC_2 for these parameters, and find no significant change in the FS.

Acknowledgements

We would like to thank G. Santi for his development of the susceptibility code, and the EPSRC (UK) for financial support.

-
- [1] J. A. Wilson, F. J. Di Salvo and S. Mahajan, Phys. Rev. Lett. **32**, 882 (1974).
 - [2] A. W. Overhauser, Phys. Rev. **128**, 1437 (1962).
 - [3] M.D. Johannes, I.I. Mazin and C.A. Howells, Phys. Rev. B **73**, 205102 (2006).
 - [4] M.D. Johannes and I.I. Mazin, Phys. Rev. B **77**, 165135 (2008).
 - [5] M. Murase, A. Tobe, H. Onodera, Y. Hirano, T. Hosaka, S. Shimomura and N. Wakabayashi, J. Phys. Soc. Jpn. **73**, 2790 (2004).
 - [6] W. Schäfer, W. Kockelmann, G. Will, J.K. Yakinthos and P.A. Kotsanidis, J. Alloys and Compounds **250**, 565 (1997).
 - [7] S. Shimomura, C. Hayashi, G. Asaka, N. Wakabayashi, M. Mizumaki and H. Onodera, Phys. Rev. Lett. **102**, 076404 (2009).
 - [8] The atomic positions used in the calculations were: R : (0, 0, 0.9936); Ni: (0.5, 0, 0.608); C: (0.5, 0.155, 0.285); C: (0.5, -0.155, 0.285).
 - [9] B. Barbiellini, S.B. Dugdale and T. Jarlborg, Comput. Mater. Sci. **28**, 287 (2003).
 - [10] L. Hedin and B.I. Lundqvist, J. Phys. C **4**, 2064 (1971).
 - [11] O. Gunnarsson and B.I. Lundqvist, Phys. Rev. B **13**, 4274 (1976).
 - [12] W. Jeitschko and M.H. Gerss, J. Less-Common Metals **116**, 147 (1986).
 - [13] H. Onodera, Y. Koshikawa, M. Kosaka, M. Ohashi, H. Yamauchi and Y. Yamaguchi, J. Magn. Magn. Mater. **182**, 161 (1998).
 - [14] J. Rath and A.J. Freeman, Phys. Rev. B **11**, 2109 (1975).
 - [15] M. Mizumaki, N. Kawamura and H. Onodera, Phys. Stat. Sol. C **3**, 2767 (2006).
 - [16] A. Subedi and D.J. Singh, arXiv:0905.0511 (2009).